Journal Name

ARTICLE TYPE

Cite this: DOI: 10.1039/xxxxxxxxxx

Towards improved magnetic fluid hyperthermia: Major-loops to diminish variations in local heating

Cristina Munoz-Menendez,*[a] David Serantes,[a,b] Juan M. Ruso,[a] and Daniel Baldomir*[a]

Received Date
Accepted Date

DOI: 10.1039/xxxxxxxxxx

www.rsc.org/journalname

In the context of using magnetic nanoparticles for heat-mediated applications, the need of an accurate knowledge of the *local* (at nanoparticle level) heat generation in addition to the usually studied *global* counterpart has been recently highlighted. Such need requires accurate knowledge of the links among intrinsic particle properties, system characteristics and experimental conditions. In this work we have investigated the role of the particles' anisotropy polydispersity in relation to the amplitude (H_{max}) of the AC magnetic field using a Monte Carlo technique. Our results indicate that it is better to use particles with large anisotropy for enhancing global heating, whereas for achieving homogeneous local heating it is better to use lower anisotropy particles. The latest ensures that most of the system undergoes major-loop hysteresis conditions, which is the key-point. This is equivalent to say that low-anisotropy particles (i.e. with less heating capability) may be better for accurate heat-mediated applications, which goes against some research trends in the literature that seek for large anisotropy (and hence heating) values.

1 Introduction

Controlling magnetic nanoparticles' (MNPs) features such as size or anisotropy is important to improve the efficacy and reduce the side effects of MNP-based biomedical applications.[1] One of these promising applications is magnetic fluid hyperthermia (MFH), where MNPs are introduced into the tumor and subjected to an external alternating magnetic field (H_{AC}) which heats them in order to kill the cancer cells.[2,3] Optimizing the heating efficiency is a main research objective in the MFH field, because this would allow to minimize the amount of MNPs necessary for the treatment.

The heating efficiency of MNPs is usually reported in terms of the *Specific Absorption Rate*, SAR, i.e. the ratio of electromagnetic energy absorbed by the MNPs. Its value is estimated either from the initial slope of the temperature variation (ΔT) *vs.* time curve or from magnetic measurements as $SAR = HL \cdot f$. HL stands for the hysteresis losses (area of the $M(H)$ cycle) and f is the frequency of the AC field.[4] Assuming a negligible contribution of Brownian rotation to heat production,[5–7] in the latter form ($SAR = HL \cdot f$) it is straightforward to see that both the size and the magnetic anisotropy of the MNPs are key heating parameters: for a random particle assembly the maximum hysteresis loop area is $\approx 2KV$, with K the particle anisotropy constant and V its volume.[8] The previous assertion is preserved as far as V falls within the range of coherent rotation for the magnetization. Therefore, the K value -**which can be tuned via shape (magnetostatic contribution), size (magnetocrystalline/surface competition) and/or composition**-, plays a crucial role to be considered when designing a MFH application.

Furthermore, the anisotropy plays an additional key-role in the MFH performance: it regulates the heating output of the particles depending on the amplitude of the AC field, H_{max}. Considering the usual definition of the anisotropy field, $H_A = 2K/M_S$ (M_S is the saturation magnetization), it can be roughly stated that, for a randomly distributed non-interacting system, the hysteresis losses will be negligible for $H_{max}/H_A <\approx 0.5$ (minor loops) and significant otherwise.[9] Of course this simplified description may change significantly if interparticle dipolar interactions cannot be neglected.[10] The double role of the anisotropy, determining the maximum HL value, and variation of the hysteresis losses with the magnetic field, is illustrated in Fig. 1: top panel (A) shows the $M(H)$ hysteresis loops of 3 different samples with the same characteristics (monodisperse, non-interacting, and same M_S and V values), the only difference being the value of K (which is also monodisperse). Obviously, the curves scale if plotting the data *vs.* the corresponding normalized H/H_A values. Complementary, the HL values (bottom panel, B) follow a very similar trend that also scales if, in addition to the H_{max}/H_A normalization, each HL data is normalized by the corresponding $2KV$ values. At low applied fields, the sample with the smallest K starts to release energy before the other ones since it has the lowest coercive field of the three systems. Also, note that the maximum normalized hystere-

[a] *Instituto de Investigacións Tecnolóxicas and Departamento de Física Aplicada, Universidade de Santiago de Compostela, 15782 Santiago de Compostela, Spain.*
[c] *Department of Physics, University of York, York YO10 5DD, U.K.*
* Corresponding author(s): cristina.munoz@usc.es, daniel.baldomir@usc.es

sis losses are equal to the anisotropy constant of the sample K. Ref. 11 shows experimentally that hysteresis losses and coercivity present a linear correlation (see the inset of Fig. 5).

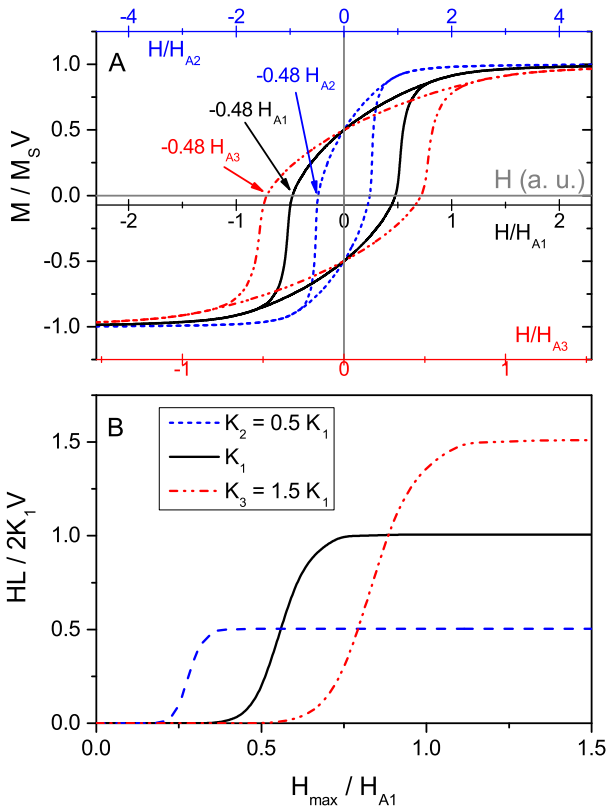

Fig. 1 A: Major hysteresis loops for three ideal monodisperse systems, with the only difference being the respective anisotropy constants: K_1, $K_2 = 0.5K_1$ and $K_3 = 1.5K_1$. B: evolution of the corresponding global hysteresis losses, HL, as a function of H_{max}. In both cases the K_1 system is used as the reference for the results. It is easy to see that if H is normalized by the H_A value of each sample (see separate x-axes of the other two samples), the scaling of both the $M(H)$ loops and the HL values is obtained.

These two key aspects of the magnetic anisotropy are well known in the MFH research field and have been intensively discussed in the literature. For example, Vallejo-Fernández and coauthors [12] interpreted the considerable variations in heating output obtained experimentally in terms of anisotropy polydispersity, considering the particle populations with different K-values. Another example can be found in our own recent work, [10] in which the role of the K vs. H_{max} in the maximum heating performance is studied also considering the relative interplay with the dipole-dipole coupling (building up the so-called *'magnetic hyperthermia trilemma'*).

There is however one additional aspect that, to the best of our knowledge, has not been reported in the literature so far and that could have important consequences for the effectiveness of MHF: *which is the role of anisotropy polydispersity regarding heat dissipation at local (nanoparticle) level*? **Note that in the present approach, by *local* we mean a set of particles inside the sample with the same characteristics (material, size, etc.). And *local heat* would be the amount of thermal energy that the set of particles can release. Studying the heat/temperature spatial or temporal variations in the nanoparticles' environment is out of the scope of this work.** Over the last few years, the study of heat dissipation at single particle level (*nm* scale) is receiving a growing attention **(see e.g. Ref. 13)**, after some works [14–16] reported cell death under an AC field with negligible *global* temperature increase. A possible explanation of these experimental results could be that the large ΔT increments observed at the particle surface -which rapidly decay only a few *nm* away- during an AC experiment, [17,18] would be enough to trigger cell apoptosis without noticeable *global* ΔT effects. These results clearly emphasize the need to investigate the heat dissipation at *local* level, in addition to the usual *global* approach. [19] Furthermore, K polydispersity is unavoidable in current synthesis techniques of MNPs, hence emphasizing the need to investigate its (double, as described above) role in MFH. This is the objective of the current work: to theoretically investigate the effect of K-polydispersity for MFH, with particular attention paid to the *local* heat dissipation aspect.

2 Model

In order to achieve the proposed objective, we have used a Monte Carlo technique to simulate $M(H)$ hysteresis loops in order to obtain the HL values under different H_{max} and K-polydispersity conditions. In our model we assume ferromagnetic-like behavior for the particles, i.e. the particles are in the blocked state (see for example Ref. 8 for a detailed description of the computational procedure).

Since size and anisotropy play a similar role regarding thermal stability, [8] we consider a size-monodisperse system in order to specifically distinguish the role of the anisotropy. The anisotropy is treated in the same way as in Ref. 12, i.e. uniaxial with a dispersion in K-values that follows a normal distribution with average $\langle K \rangle$ and standard deviation σ_K:

$$f(K;\langle K\rangle,\sigma_K) = \frac{1}{\sqrt{2\pi}\sigma_K} e^{-\frac{(K-\langle K\rangle)^2}{2\sigma_K^2}}. \quad (1)$$

Both the easy-axes orientations and the particle positions are randomly distributed. The uniaxial-anisotropy assumption follows previous works [12,20] based on magnetite nanoparticles for **MFH** applications. Magnetite has cubic (and negative) magnetocrystalline anisotropy, but its value is relatively small. Hence, shape-anisotropy effects due to deviations from sphericity result in extra anisotropy terms that may dominate over the cubic one. Thus, considering regular ellipsoid shape for simplicity, it has been shown that small deviations from sphericity (aspect ratios above $1.1-1.2$) quickly result in domination of the uniaxial *shape* anisotropy term over the cubic one. [12,20] Therefore, the anisotropy of the particle can be *effectively* described by its uniaxial value arising from shape effect. This is illustrated by the insets in Fig. 2, where ellipsoidal particles of different aspect ratios stand for different K values. Note that for a rigurous treatment it would be necessary to take into account both cubic and uniaxial contributions, [21–25] and also other more complex shapes. [26] However, for the objective of the present work, the origin of the K polydispersity or its type is not a main issue, hence we just assume

it to be defined by Eq. (1) regardless of its physical origin.

In the computational treatment, we have grouped the particles in anisotropy categories of value K_j to take into account the distribution of K values. From here on, when talking about anisotropy categories, we will be referring to K_j or to the normalized parameter $\frac{K_j}{\langle K \rangle}$. This normalized parameter may sometimes give a more intuitive value of the difference of a given category with respect to the average system. Note that since we are assuming a normal distribution, $\langle K \rangle$ is the same regardless of the σ value.

3 Results

The first step towards understanding the role of K-polydispersity in the heating performance of MNPs at *local* level will be to understand the global dissipated energy as a function of the K and H_{max} values. Fig. 2 shows the influence of the applied field for three systems having the same average anisotropy constant $\langle K \rangle$ but different standard deviations σ_K in their anisotropy constant distributions. The monodisperse case $\sigma_K = 0$ has been included as a reference. If σ_K increases, there will be more particles with a coercive field lower than the applied field H. Therefore, a small H_{max} will be enough to dissipate energy. If the applied field is high enough so that all the particles of the sample are blocked, polydispersity in K does not affect the global hysteresis losses (assuming the same macroscopic anisotropy constant). The insets show the equivalence between the anisotropy constant distributions and the shape of the particles in this work: having no anisotropy is equivalent to have a spherical particle whereas increasing it means going towards a spheroid with an aspect ratio smaller than one.

Fig. 3A shows the evolution of the global hysteresis losses for the three samples with different σ_K of Fig. 2 with the amplitude of the applied magnetic field. Three different regions can be differentiated depending on the effect of σ_K and $H_{max}/\langle H_A \rangle$ on the **global** hysteresis losses: there will be more released energy at low fields, $H_{max} < 0.5\langle H_A \rangle$, if the sample is polydisperse. The contrary will occur at larger fields, $0.5\langle H_A \rangle < H_{max} < 1.0\langle H_A \rangle$. As previously seen, the anisotropy distribution is unimportant for the global hysteresis losses if the applied field is big enough to ensure the saturation of all the particles, $H_{max} > 1.0\langle H_A \rangle$. The reason for this is depicted in Fig. 3B, where the anisotropy constants distribution is used to show which anisotropy categories are contributing to heating at the three marked applied fields. Broadening the distribution enables to have dissipation at lower applied fields although this released energy will be less for the polydisperse case if the field is higher. The percentage of particles of the sample releasing energy is also indicated.

To illustrate the usefulness of our results for interpreting experimental data, we next discuss Fig. 3 in relation to some apparently unexpected SAR values reported in the literature. High SAR values up to ≈170 W/g have been measured for $MnFe_2O_4$ nanoparticles[27], whereas much lower ones, up to ≈30 W/g, have been reported for $CoFe_2O_4$[27] and Fe_3O_4 nanoparticles[28] at $H_{max} \approx 200$ Oe. These values may seem surprising at first if considering the direct proportionality between SAR and anisotropy[10], because the effective anisotropy constant of $CoFe_2O_4$ and Fe_3O_4 is in the range of $10^5 J/m^3$

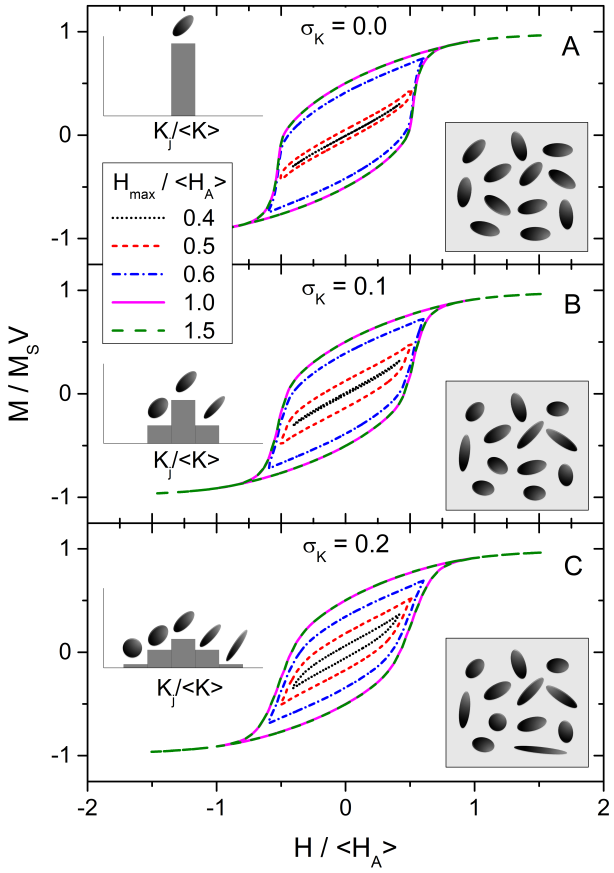

Fig. 2 Influence of the applied field on the global hysteresis cycles for different degrees of anisotropy polydispersity: A monodisperse, B $\sigma_K = 0.1$ and C $\sigma_K = 0.2$. Each M(H) curve is done for a different value of H_{max}. Insets: link between the local K_j values and the shape of the particles.

whereas the one of $MnFe_2O_4$ is in the range of $10^3 J/m^3$. Therefore, one could expect that the $MnFe_2O_4$ nanoparticles would dissipate much less than the other ones. However, when the ratio H_{max}/H_A is analyzed, it appears that this ratio is very close to 1 in the case of $MnFe_2O_4$ nanoparticles (≈0.9) and much lower (<0.2) for the $CoFe_2O_4$ and Fe_3O_4 ones. Fig. 3 suggests that the $MnFe_2O_4$ sample may be highly saturated (major loop conditions), with most of the particles releasing energy; whereas only the particles with the lowest anisotropies would be contributing to heat dissipation in the case of $CoFe_2O_4$ and Fe_3O_4 samples (minor loop conditions for most of the particles within the system).

The importance of local heating **(at individual nanoparticle level)**, which is clear from Fig. 3, is systematically analyzed in detail for the different anisotropy polydispersity conditions and field amplitudes. The results are reported in Fig. 4, which shows the evolution of the local HL values as a function of the applied field for the two values of σ_K previously considered. The global hysteresis losses are indicated with a black solid line for each case. Since $\langle K \rangle = K_0$, (K_0 is the anisotropy constant for the monodisperse system) the blue dashed lines represent the hysteresis losses of the monodisperse case. The difference between the global hysteresis losses for the monodisperse case and the

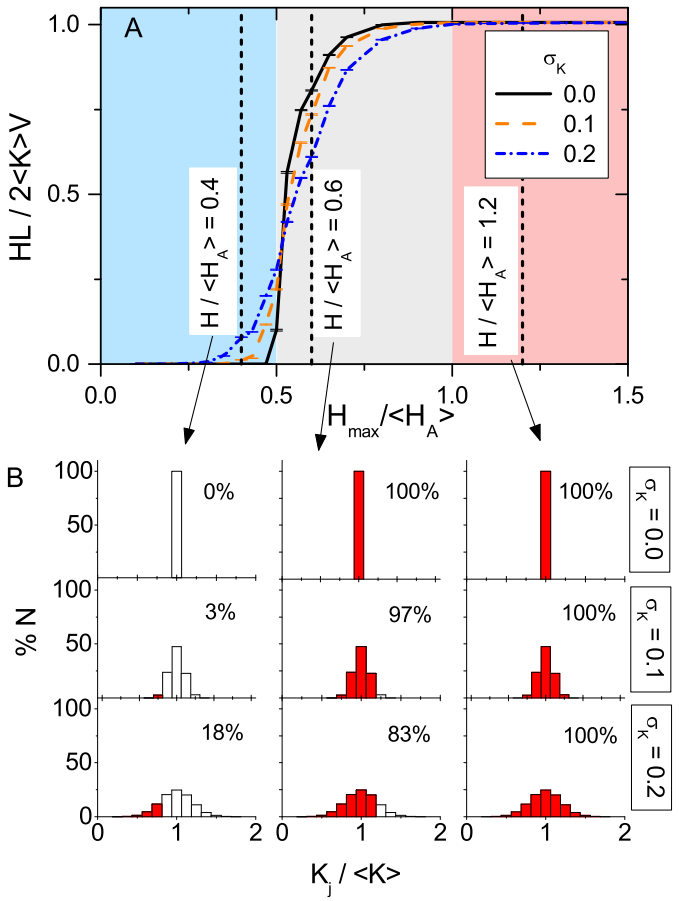

Fig. 3 A: Evolution of the global hysteresis losses for $\sigma_K = 0.0$, 0.1 and 0.20. The 3 shaded regions represent different effects of anisotropy polydispersity and applied field on the global hysteresis losses. B: Distribution of anisotropy constants where the y-axis represents the percentage of particles belonging to each anisotropy category. The red filled bars show which anisotropy categories are contributing to the heating for each σ_K and for the three selected applied fields. The percentage of particles of the sample releasing energy is also indicated.

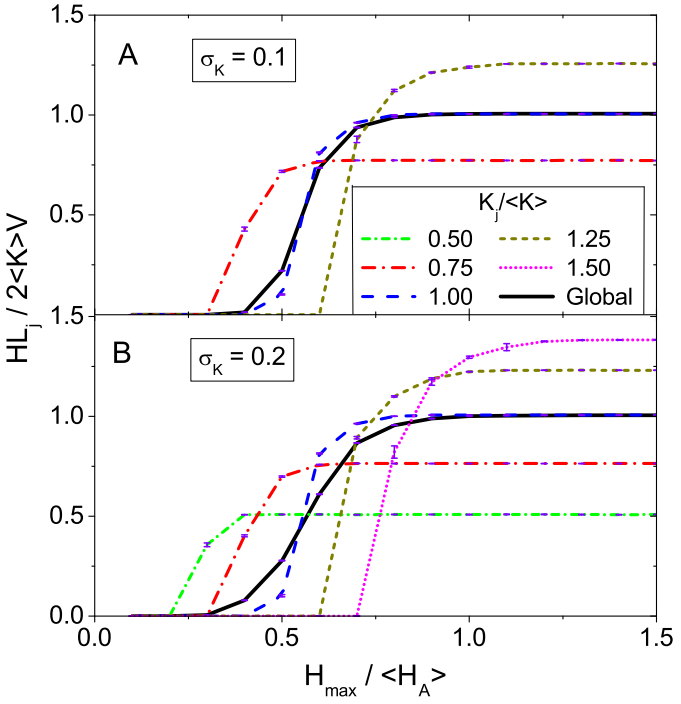

Fig. 4 Evolution of the local hysteresis losses for different categories K_j as a function of the normalized applied field for two values of σ_K: A 0.10 and B 0.20. The black solid line stands for the global hysteresis losses. The blue dashed line also represents the hysteresis losses of the monodisperse case $\langle k \rangle = 1$.

polydisperse one increases with σ_K, as previously seen. When all the sample is saturated, both lines are coincident since the distribution of anisotropy is normal. With increasing applied field, the hysteresis loop opens later and saturation is achieved later for larger K_j values. When the applied field is large enough to open the cycles of the particles with higher anisotropy, their hysteresis losses are also greater.

Fig. 5 shows the normalized hysteresis losses of each category K_j for different applied fields taking into account the number of particles that each category has. The inset shows the normalized hysteresis losses of each category, but per particle. As Fig. 3B indicated, increasing the amplitude of the applied field allows particles with bigger K_j to dissipate. As expected from a saturated system $H_{max} > 1.0\langle H_A \rangle$ where all the particles can dissipate as much as they anisotropy constant allows them, the relationship between K_j and the released energy HL_j fulfills $HL_j = 2K_jV$. This fact is represented by the green dashed line of the inset. If looking at the inset, one may think that certain categories are responsible for most part of the dissipation. However, when looking at the main graph of Fig. 5, it is seen that the actual number of particles may change the K_j categories having more weight regarding energy dissipation. This difference is clearly seen for the smallest and the biggest field amplitudes.

To see how much the normalized local hysteresis losses $\frac{HL_j}{2\langle K \rangle V}$ deviate from the normalized global ones $\frac{HL}{2\langle K \rangle V}$ in average for each applied magnetic field, the parameter σ_{HL} can be used. It is calculated as a standard deviation:

$$\sigma_{HL} = \sqrt{\frac{1}{N}\sum_{j=1}^{P} N_j \left(\frac{HL_j}{2\langle K \rangle V} - \frac{HL}{2\langle K \rangle V} \right)^2}. \qquad (2)$$

P is the maximum number of categories. Taking the quotient $\frac{\sigma_{HL}}{HL/2\langle K \rangle V}$ instead of σ_{HL} makes easier to compare the deviation of the local hysteresis losses for different applied fields. It is not the same having a big σ_{HL} value when the global hysteresis losses are big or when they are small. The heating dispersion would be more important in the second case. Fig. 6 demonstrates this for the case of $\sigma_K = 0.20$. The left axis represents the evolution of the σ_{HL} values with the field, whereas the right axis refers to the $\frac{\sigma_{HL}}{HL/2\langle K \rangle V}$ value. It has been expressed as a percentage to ease the reading of the data. Therefore, the standard deviation is small at low applied fields, but since the global losses are small too, they have a great effect. However, at high fields the standard deviation is higher, but the global hysteresis losses as well, so the local dissipation is not very important. Fig. 6 suggests that it is better to choose a material that has an anisotropy constant which allows the material to already be saturated when it is subjected

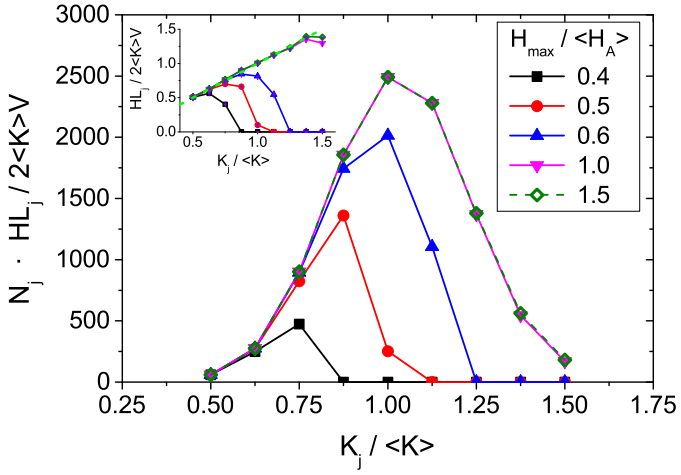

Fig. 5 Normalized local hysteresis losses multiplied by the number of particles in each size category N_j. The figure shows the size categories actually dissipating energy because the amount of energy released will depend on the amount of particles as well. The inset shows the dependence of the normalized local hysteresis losses per particle with K_j. The dependence is linear for the case of maximum hysteresis losses.

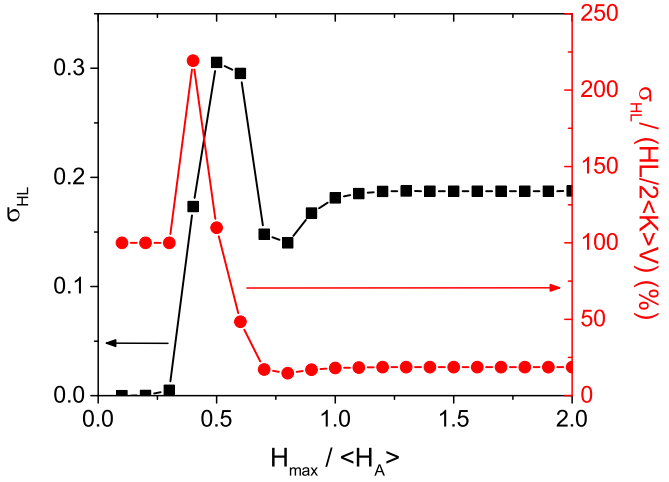

Fig. 6 Left axis: Standard deviation of the local normalized hysteresis losses as a function of the applied field. Right axis: Percentage of this standard deviation in relation to the normalized global hysteresis losses. The effect of the deviation depends on the reference value considered. σ_K is 0.20.

to a typical hyperthermia magnetic field.

4 Conclusion

We have proved that the magnetic anisotropy constant K and its dispersion σ_K play an important role regarding global and local energy dissipation in MFH, not only because energy release is proportional to K but also because it regulates the heating output depending on the amplitude of the applied magnetic field H_{max}. At a low amplitude of the applied field, $H_{max} < 0.5\langle H_A\rangle$, a more polydisperse sample will dissipate more energy because the particles with the lowest anisotropy will have a coercive field smaller than the applied field. If the amplitude of the magnetic field increases, $0.5\langle H_A\rangle H_{max} < 1.0\langle H_A\rangle$, the sample less polydisperse will release more energy since the particles with bigger anisotropy will be able to dissipate energy and this energy is proportional to the K-values. In case that the applied field is big enough to saturate all the sample, $H_{max} > 1.0\langle H_A\rangle$, the difference between having a bigger or smaller σ_K will be only appreciated at local level. **At this point, we would like to draw attention to the recent experimental work of Sanz and coauthors**[29], where they showed that MFH decreased cell viability more than immersing the sample in a water bath at the same global target temperature, associating this to local heating effects. **Our results show that K and σ_K, which are linked to different particle shapes in the sample, affect both global and local energy dissipation. Since their samples are polydisperse in shape, thus also in anisotropy, our results may be one possible explanation for their findings.**

We also showed that to ensure local energy dissipation as homogeneous as possible, it is better to use an applied field which allows major loop conditions. Having a saturated sample does not imply homogeneous local energy release because particles with higher anisotropy K_j will dissipate more, but the key point is to tune the anisotropy of the sample K and the amplitude of the applied field H_{max} to dissipate in the desired energy range with the less local heat dispersion as possible. In other words, given that anisotropy polydispersity is unavoidable and energy dissipation is proportional to K and H_{max}, a sample with a lower K should be chosen for this purpose if the amplitude of the applied field had an upper limit. The other way around, if a specific material is necessary (fixed K), a higher H_{max} would be preferable.

Acknowledgments

The authors thank the Centro de Supercomputación de Galicia (CESGA) for the computational facilities. This work was co-financed by the Spanish MINECO (Project MAT2013-47078-C2-2-P), Xunta de Galicia, Spain (Project GRC 2014/013, 'Programa de axudas á etapa predoutoral' and financial support of D.S. under Plan I2C) and 'Fondo Social Europeo 2014/2020'.

References

1 M. Colombo, S. Carregal-Romero, M. F. Casula, L. Gutierrez, M. P. Morales, I. B. Boehm, J. T. Heverhagen, D. Prosperi and W. J. Parak, *Chem. Soc. Rev.*, 2012, **41**, 4306–4334.

2 P. Tartaj, M. P. Morales, S. Veintemillas-Verdaguer, T. González-Carreño and C. J. Serna, *J. Phys. D: Appl. Phys.*, 2003, **36**, R182.

3 D. Ortega and Q. A. Pankhurst, *Nanoscience: Volume 1: Nanostructures through Chemistry*, The Royal Society of Chemistry, 2013, vol. 1, pp. 60–88.

4 E. A. Périgo, G. Hemery, O. Sandre, D. Ortega, E. Garaio, F. Plazaola and F. J. Teran, *Appl. Phys. Rev.*, 2015, **2**, 041302.

5 S. Dutz, M. Kettering, I. Hilger, R. Müller and M. Zeisberger, *Nanotechnology*, 2011, **22**, 265102.

6 R. Di Corato, A. Espinosa, L. Lartigue, M. Tharaud, S. Chat, T. Pellegrino, C. Ménager, F. Gazeau and C. Wilhelm, *Biomaterials*, 2014, **35**, 6400–6411.

7 Hence, the only energy dissipation mechanism is Néel reversal, i.e. the reorientation of the particles' magnetization over their energy barriers.

8 C. Munoz-Menendez, I. Conde-Leboran, D. Baldomir, O. Chubykalo-Fesenko and D. Serantes, *Phys. Chem. Chem. Phys.*, 2015, **17**, 27812–27820.

9 S. Hergt, S. Dutz, R. Müller and M. Zeisberger, *J. Phys.: Condens. Matter*, 2006, **18**, S2919–S2934.

10 I. Conde-Leboran, D. Baldomir, C. Martinez-Boubeta, O. Chubykalo-Fesenko, M. P. Morales, G. Salas, D. Cabrera, J. Camarero, F. J. Teran and D. Serantes, *J. Phys. Chem. C*, 2015, **119**, 15698–15706.

11 S. Dutz, R. Hergt, J. Mürbe, R. Müller, M. Zeisberger, W. Andrä, J. Töpfer and M. E. Bellemann, *J. Magn. Magn. Mater.*, 2007, **308**, 305–312.

12 G. Vallejo-Fernandez and K. O'Grady, *Appl. Phys. Lett.*, 2013, **103**, 142417.

13 R. P. Tan, J. Carrey and M. Respaud, *Phys. Rev. B*, 2014, **90**, 214421.

14 M. Creixell, A. C. Bohorquez, M. Torres-Lugo and C. Rinaldi, *ACS Nano*, 2011, **5**, 7124–7129.

15 L. Asin, M. Ibarra, A. Tres and G. Goya, *Pharm. Res.*, 2012, **29**, 1319–1327.

16 A. Villanueva, P. De La Presa, J. M. Alonso, T. Rueda, A. Martinez, P. Crespo, M. Morales, M. A. Gonzalez-Fernandez, J. Valdes and G. Rivero, *J. Phys. Chem. C*, 2010, **114**, 1976–1981.

17 A. Riedinger, P. Guardia, A. Curcio, M. A. Garcia, R. Cingolani, L. Manna and T. Pellegrino, *Nano Lett.*, 2013, **13**, 2399–2406.

18 J. T. Dias, M. Moros, P. del Pino, S. Rivera, V. Grazú and J. M. de la Fuente, *Angew. Chem.*, 2013, **125**, 11740–11743.

19 C. Munoz-Menendez, I. Conde-Leboran, D. Serantes, R. Chantrell, O. Chubykalo-Fesenko and D. Baldomir, *Soft Matter*, 2016, **12**, 8815–8818.

20 N. A. Usov, S. A. Gudoshnikov, O. N. Serebryakova, M. L. Fdez-Gubieda, A. Muela and J. M. Barandiarán, *J. Supercond. Novel Magn.*, 2013, **26**, 1079–1083.

21 V. Russier, C. De-Montferrand, Y. Lalatonne and L. Motte, *J. Appl. Phys.*, 2013, **114**, 143904.

22 S. Noh, W. Na, J. Jang, J. Lee, E. J. Lee, S. H. Moon, Y. Lim, J. Shin and J. Cheon, *Nano Lett.*, 2012, **12**, 3716–3721.

23 C. Martinez-Boubeta, K. Simeonidis, A. Makridis, M. Angelakeris, O. Iglesias, P. Guardia, A. Cabot, L. Yedra, S. Estradé, F. Peiró *et al.*, *Scientific reports*, 2013, **3**,.

24 H. Khurshid, J. Alonso, Z. Nemati, M. H. Phan, P. Mukherjee, M. L. Fdez-Gubieda, J. M. Barandiarán and H. Srikanth, *J. Appl. Phys.*, 2015, **117**, 17A337.

25 M. J. Correia, W. Figueiredo and W. Schwarzacher, *Phys. Lett. A*, 2014, **378**, 3366–3371.

26 R. Das, J. Alonso, P. Z. Nemati0, V. Kalappattil, D. Torres, M. Phan, E. Garaio, J. A. García, J. L. Sanchez-Llamazares and H. Srikanth, *J. Phys. Chem. C*, 2016, **120**, 10086–10093.

27 M. M. Cruz, L. P. Ferreira, J. Ramos, S. G. Mendo, A. F. Alves, M. Godinho and M. D. Carvalho, *J. Alloys Compd.*, 2017, **703**, 370–380.

28 G. Vallejo-Fernandez, O. Whear, A. G. Roca, S. Hussain, J. Timmis, V. Patel and K. O'Grady, *J. Phys. D: Appl. Phys.*, 2013, **46**, 312001.

29 B. Sanz, M. P. Calatayud, T. E. Torres, M. L. Fanarraga, M. R. Ibarra and G. F. Goya, *Biomaterials*, 2017, **114**, 62–70.